Soft Matter

RSC Publishing

PAPER

View Article Online
View Journal | View Issue

Cite this: *Soft Matter*, 2013, **9**, 3976

Monte Carlo simulations of a polymer confined within a fluid vesicle

Miha Fošnarič,[a] Aleš Iglič,[a] Daniel M. Kroll[b] and Sylvio May*[b]

Monte Carlo simulations are employed to study a fluid vesicle that contains a single worm-like polymer chain. The contour length of the polymer is about five times the circumference of the nominally spherical vesicle. We vary the degree of polymer confinement in our simulations by increasing the persistence length of the polymer. The vesicle is represented by a randomly triangulated self-avoiding network that can undergo bending deformations. Upon increasing the persistence length of the polymer beyond the size of the vesicle, we observe a transition of the polymer from an isotropic disordered random conformation to an ordered toroidal coil. Concomitantly, the vesicle adopts an oblate shape to allow for some expansion of the polymer coil inside the vesicle. It is convenient to characterize both polymer and vesicle in terms of the asphericity, a quantity derived from the gyration tensor. At the onset of the polymer's ordering transition, the asphericity passes through a minimum for both polymer and vesicle. The increase in vesicle asphericity for a semi-flexible polymer can be understood in terms of ground state energy calculations, either for a simplified representation of the vesicle shape (we specifically discuss a disk shape with a semi-toroidal rim) or involving a full vesicle shape optimization. The asphericity of the polymer coil results from conformational fluctuations and can be rationalized using Odijk's deflection length of strongly curved semi-flexible polymers.

Received 22nd December 2012
Accepted 14th February 2013

DOI: 10.1039/c3sm27938c

www.rsc.org/softmatter

1 Introduction

Polymers are often confined to spaces much smaller then their natural size.[1–3] This is routinely encountered for the packaging of nucleic acids in viruses,[4] the transport of biopolymers through nanopores,[5–7] or in industrial applications such as fractionation methods using microfluidic devices.[8,9] The confinement boundaries are not necessarily rigid; soft boundaries may adapt their shape so as to more favorably accommodate the enclosed polymers. Such structural variability is often implied by the flexibility of cellular boundaries and sub-cellular structures.[10] For example, marginal microtubule bands in some animal red blood cells help them to obtain their physiological oblate shapes,[11–13] whereas sickle hemoglobin fibers rigidify human red blood cells into pathological prolate shapes.[14] In artificial lipid vesicles, different types of polymers may be self-assembled,[15,16] reconstituted[17] or entrapped,[2,18,19] strongly influencing vesicle shape and properties. Conversely, membrane properties can affect the conformation of vesicle-encapsulated biopolymers.[20] Actin filaments have also been polymerized and confined into phospholipid-stabilized emulsion droplets.[21]

Confinement of polymers within closed surfaces has been modeled extensively using both simulations and theory.[22] This includes the confinement of linear or ring-like[23,24] polymers into cavities[25,26] (often for cavities of fixed spherical[27,28] or cylindrical[29,30] shape), or their surfaces.[31,32] It also includes soft confining boundaries such as globular and tubular lipid membranes.[33] Specifically, we mention work of Marenduzzo and Orlandini[34] who simulated the growth of a self-assembling semi-flexible polymer inside a soft vesicle. It was shown (i) that very stiff polymers stall growth and lock the vesicle into a deformed prolate shape (similar to fibers in sickle red blood cells[14]), (ii) that polymers with intermediate stiffness form a toroidal configuration which distorts the membrane into an oblate shape (like marginal microtubule bands in growing erythrocytes[11,12]), and (iii) that more flexible polymers grow long inside the vesicle, forming massive spool-like condensates, inflating the vesicle isotropically (like genome packing in the cell nucleus or bacteria[1]).

In this work we consider a fluid-like lipid vesicle that encloses a single polymer of fixed contour length. We choose the contour length to be about five times the circumference of the vesicle if adopting a spherical shape. The vesicle represents a cavity that – unlike a rigid spherical confinement – is responsive and can adapt to the preferred shape of the polymer. Both polymer and vesicle shapes are governed by their respective bending elastic energies and entropic contributions. We model the polymer as a worm-like chain and the vesicle as a

[a]*Laboratory of Biophysics, Faculty of Electrical Engineering, University of Ljubljana, Tržaška 25, 1000 Ljubljana, Slovenia*

[b]*Department of Physics, North Dakota State University, Fargo, ND, 58108-6050, USA. E-mail: sylvio.may@ndsu.edu*

closed fluid sheet that resists bending. Our work attempts to characterize equilibrium properties of the vesicle–polymer system using phenomenological modeling and computer simulations. We are particularly interested in the question how the vesicle accommodates the polymer and how the polymer affects the vesicle shape. To this end, we systematically vary the intrinsic persistence length ξ of the polymer from values much smaller to values much larger than the vesicle size. Specifically, in Section 2 we investigate the *ground state* (*i.e.*, the state of minimal energy when neglecting thermal fluctuations) of the vesicle–polymer system using approximative geometrical models and numerical vesicle shape optimization. Monte Carlo simulations are employed in Section 3 to describe thermal fluctuations of the vesicle and the polymer. In our simulations we represent the vesicle as a randomly triangulated surface.[35,36] Upon increasing the stiffness of the polymer we observe a transition from an isotropic disordered random structure to an ordered toroidal coil. Concomitantly, the vesicle undergoes a transition from an (almost) spherical to an oblate disk-like shape, accommodating the toroidal coil close to its waist. We characterize the vesicle and polymer in terms of their asphericity; see Section 4. Appendices 1 and 2 contain technical details of the phenomenological models and shape optimization, respectively.

2 Ground state calculation

Consider a fluid-like lipid vesicle of fixed surface area $A_{\mathrm{ves}} = 4\pi {R_0}^2$, where R_0 is the radius of a corresponding sphere with the same area. The vesicle contains a single linear worm-like polymer chain of fixed contour length L with $L \gg R_0$. (In the present work we shall focus on one specific case, $L/(2\pi R_0) \approx 5$.) The elastic energy of the vesicle–polymer system,

$$E = \frac{\kappa}{2} \int_{A_{\mathrm{ves}}} (c_1 + c_2)^2 \, \mathrm{d}a + \frac{\xi k_{\mathrm{B}} T}{2} \int_L c^2 \, \mathrm{d}l \qquad (1)$$

contains two bending contributions, the first from the vesicle and the second from the polymer. The first integration in eqn (1) runs over the vesicle surface, where c_1 and c_2 denote the two principle curvatures and κ is the bending stiffness.[37] For a vesicle that consists of a symmetric membrane (including the absence of a mismatch between the lateral areas of the two individual membrane leaflets) and does not change its topology, we need to include neither a spontaneous curvature nor a Gaussian bending contribution. The second integration in eqn (1) runs over the contour of the polymer, with L being the contour length, c the local curvature, and $\xi k_{\mathrm{B}} T$ the bending stiffness of the polymer. The latter is expressed in terms of the intrinsic persistence length ξ of the polymer and the thermal energy $k_{\mathrm{B}} T$ (where k_{B} is Boltzmann's constant and T the absolute temperature).

We first discuss the ground state and corresponding ground state energy of our vesicle–polymer system. If the polymer is infinitely rigid, $\xi/R_0 \to \infty$, the ground state must correspond to a fully stretched polymer residing within an extended, tube-like vesicle. Reducing the polymer stiffness allows the length of the extended tube to relax. This can be described phenomenologically by modeling the tube as a sphero-cylinder – a cylinder capped by two identical hemispheres – that encloses a helical polymer; see Fig. 7 in Appendix 1 or the scheme "tube" in Fig. 1 for a fully stretched polymer. Such a model introduces the tube length as single degree of freedom for given parameters $\xi k_{\mathrm{B}} T/(\kappa R_0)$ and L/R_0. Maximal and minimal tube lengths correspond to the fully stretched polymer residing in an extended sphero-cylinder and to the polymer forming a circular ring at the equatorial region inside a spherical vesicle, respectively. Examination of the total elastic free energy as function of the tube length (see Appendix 1 for details) reveals two minima, $E = E_{\mathrm{min}}$, corresponding to maximal and minimal tube lengths. Both minima are displayed in Fig. 1 as function of $\xi k_{\mathrm{B}} T/(\kappa R_0)$ for fixed $L/(2\pi R_0) = 4.9$ (see the thin solid line marked "tube" and the dotted red line marked "sphere"). The constant value of E_{min} for the extended tube signifies the fully stretched polymer not changing its elastic energy as function of ξ. Similarly, the linear change of E_{min} for the spherical vesicle simply reflects the bending contribution of the polymer, with $E_{\mathrm{min}} \sim \xi$ for all other quantities being fixed. Fig. 1 indicates that, as $\xi k_{\mathrm{B}} T/(\kappa R_0)$ is lowered, the energetically favorable state switches discontinuously from an almost fully extended thin tube to a spherical vesicle. However, at this point (*i.e.*, at $\xi k_{\mathrm{B}} T/(\kappa R_0) \approx 90$ in Fig. 1) the two favorable states are separated by a large energy barrier. The height of the barrier is calculated in Appendix 1 for helical polymer conformations;[34,38] allowing for other polymer conformations may somewhat lower barrier, but not remove it. Hence, if trapped in an initially spherical vesicle, the polymer will be

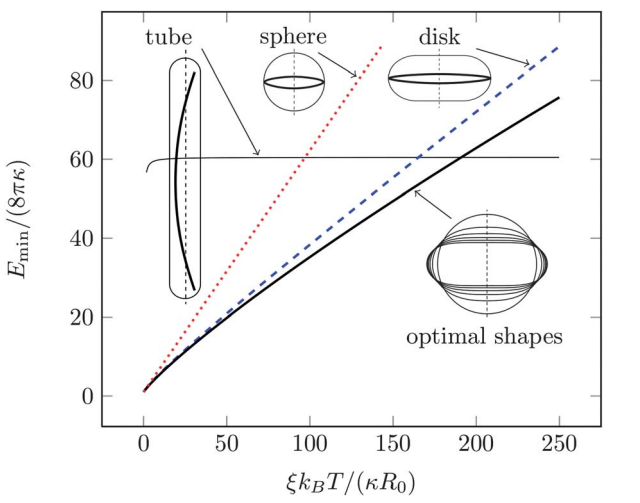

Fig. 1 Minimal total elastic energy of the vesicle–polymer system as function of the scaled polymer stiffness $\xi k_{\mathrm{B}} T/(\kappa R_0)$. The scaled polymer length in the plot is $L/(2\pi R_0) = 4.9$, corresponding to our Monte Carlo simulations in Section 3. The minimal elastic energies for various models are displayed together with an illustration of the corresponding vesicle and polymer shape: sphero-cylinder (thin solid line, marked "tube"), sphere (dotted red line, marked "sphere"), semi-toroidal disk (dashed blue line, marked "disk"), and optimized vesicle shape (thick solid line, marked "optimal shapes"). The optimal shapes are calculated as outlined in Appendix 2. They are calculated for $\xi k_{\mathrm{B}} T/(\kappa R_0) = 0$, 2, 4, 6, 8 and 10, with the corresponding radii $1.0 \times R_0$, $1.12 \times R_0$, $1.16 \times R_0$, $1.22 \times R_0$ and $1.23 \times R_0$ at the vesicle waist, respectively.

unable to adopt its fully stretched conformation through thermal fluctuations, even if full stretching corresponds to lower elastic energy of the vesicle–polymer system.

Instead of forming an extended tube-like structure, the vesicle can deform into an oblate disk-like shape, with the polymer adopting a circular ring structure at the waist of the vesicle. We can phenomenologically model the vesicle as a disk with a semi-toroidal rim. This structure, to which we refer as *disk model*, is illustrated and marked "disk" in Fig. 1. The disk model exhibits one single degree of freedom, given the parameter $L\xi k_BT/(R_0^2\kappa)$ is fixed. Analysis of the elastic free energy E (see Appendix 1 for details) reveals the presence of only one single minimum $E = E_{min}$. This minimum is depicted in Fig. 1 as function of $\xi k_BT/(\kappa R_0)$, again for fixed $L/(2\pi R_0) = 4.9$ (see the dashed blue line). It is lower than the minimum of the polymer enclosed in a sphere. Because no energy barrier resists the transformation from the spherical to the disk-like vesicle, the former is always unstable in favor of the latter.

Representing the vesicle by a flat disk with a semi-toroidal rim still overestimates the ground state energy E_{min}. Indeed, a full optimization of the vesicle shape (see Appendix 2 for details) reveals a further decrease of E_{min}. Fig. 1 displays E_{min} as function of $\xi k_BT/(\kappa R_0)$; see the thick solid line marked "optimal shapes". Fig. 1 also shows a sequence of optimized shapes, computed for various values of $\xi k_BT/(\kappa R_0)$ ranging from 0 to 10. To go beyond ground state calculations requires us to account for fluctuations, both in vesicle shape and polymer conformations. This is achieved using Monte Carlo simulations as described in the following section.

3 Monte Carlo simulations

The fluid vesicle is represented by a set of N vertices that are linked by tethers of variable length l so as to form a closed, randomly triangulated, self-avoiding network.[35,36] The lengths of the tethers can vary between a minimal value, l_{min}, and a maximal value, l_{max}. Self-avoidance of the network is ensured by choosing $l_{max}/l_{min} < \sqrt{3\left(1-(s/l_{min})^2\right)}$ where s is the maximal random displacement of the vertex. In our simulations we choose $s/l_{min} = 0.15$ and $l_{max}/l_{min} = 1.67$. The randomly triangulated network acquires its lateral fluidity from a bond flip mechanism. A single bond flip involves the four vertices of two neighboring triangles. The tether connecting the two vertices in diagonal direction is cut and reestablished between the other two, previously unconnected, vertices.

The polymer inside the vesicle is represented by M vertices that form a linear chain. The maximal vertex displacement and the maximal bond length between two neighboring vertices are chosen to be the same as for the triangulated network of the vesicle. We also introduce a minimal distance between any two polymer and vesicle vertices larger than l_{min} to ensure that the polymer cannot penetrate into the vesicle membrane. Most of our simulations are carried out without self-avoidance of the polymer; for some simulations (where specified explicitly) self-avoidance of the polymer is implemented by imposing a minimal distance l_{min} between all pairs of vertices of the polymer (and not only between neighboring vertices, as for a polymer without self-avoidance). We note that the neglect of self-avoidance renders entanglement and knot formation of the polymer irrelevant. Knots appeared sporadically in simulations with polymer self-avoidance – the corresponding runs were then discarded without further analysis.

The microstates of the vesicle–polymer system are sampled according to the Metropolis algorithm with the energy for a given microstate specified in eqn (1). The bending energy of the discretized vesicle (*i.e.*, of the triangulated network) is calculated as described by Gompper and Kroll;[35,36] for a recent review, see Ramakrishnan *et al.*[39] The bending energy of the discretized polymer is calculated according to $k_BT(\xi/\bar{l})\sum_i(1-\cos\theta_i)$, where θ_i denotes the angle between two successive bond vectors along the polymer and where the sum runs over all neighboring pairs of bond vectors; $\xi/\bar{l}$ is the persistence length, measured in units of the average bond length of the polymer, $\bar{l} \approx (l_{min} + l_{max})/2$. The starting configuration in all simulations is an almost spherical vesicle with the polymer adopting a random coil inside the vesicle.

In all our simulations the vesicle membrane is triangulated using $N = 1447$ vertices, forming $2(N-2) = 2890$ triangles. Such a vesicle, if spherical, has a radius $R_0/l_{min} \approx 13$. For the bending stiffness of the vesicle we use $\kappa = 10k_BT$. The polymer inside the vesicle consists of $M = 300$ vertices, with an average contour length, $L \approx M\bar{l}$, about 5 times longer than the circumference $2\pi R_0$ of the spherical vesicle.

Fig. 2 shows snapshots of typical equilibrium configurations for $\xi = 0$ and $\xi = R_0$. For vanishing persistence length (see the two upper images of Fig. 2) the polymer behaves almost as a random coil (although not completely, since it is still confined by the vesicle to some extent as will be discussed in Section 4).

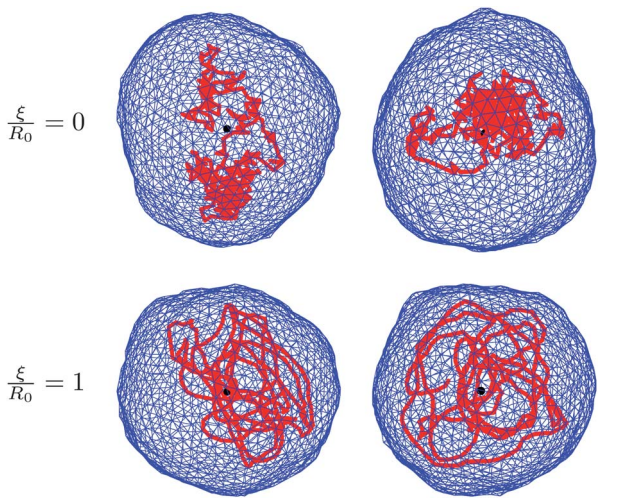

Fig. 2 Snapshots of typical equilibrium configurations of a vesicle (blue color) containing a linear polymer (red color). Each of the two rows corresponds to a scaled persistence lengths ξ/R_0 of the polymer as indicated; the two images in each row show the same system (*i.e.*, the same microstate) from two different viewpoints. The vesicle has a bending stiffness $\kappa = 10k_BT$, and the polymer has a scaled length $L/(2\pi R_0) \approx 4.9$. The polymer is modeled without accounting for self-avoidance. The black dot denotes the center of mass of the vesicle–polymer system.

Increase of the polymer stiffness so as to match the radius R_0 of the spherical vesicle results in the polymer filling the volume of the vesicle more uniformly; see the two lower images of Fig. 2. If the persistence length of the polymer increases beyond the dimensions of the vesicle, there is a transition to a more ordered structure, where the polymer forms a toroidal coil within an oblate-shaped vesicle. Corresponding snapshots are displayed in Fig. 3 for $\xi = 5R_0$ (upper images) and $\xi = 20R_0$ (lower images). An even further increase of the polymer's persistence length ξ/R_0 leads to further flattening of the disk-like vesicle, with the polymer adopting a larger ring-like shape close to the waist of the vesicle. A snapshot for $\xi = 200R_0$ is shown in Fig. 4. Here, the two rows refer to a polymer without (upper row of Fig. 4) and with (lower row of Fig. 4) self-avoidance. Self-avoidance of the polymer is manifested by the somewhat thicker coil structure but has little impact on the vesicle shape. We also note the non-vanishing angle the terminal segment of the polymer makes with the vesicle boundary – this angle is universal (*i.e.*, it does not depend on the specific material properties) and adopts a value of 24.1 degrees in the ground state.[40,41]

For a more quantitative description of the polymer-induced shape changes, the following section introduces and analyzes the asphericity of the vesicle and polymer.

4 Asphericity

The transition of the polymer from an isotropic random conformation to an ordered coil and the subsequent flattening of the vesicle shape can be characterized conveniently in terms of the *asphericity A*. To this end, we make use of the Gyration tensor, whose components are defined for a discrete object through

$$S_{ij} = \frac{1}{N}\sum_{k=1}^{N} r_{k,i} r_{k,j} \quad (i,j = 1,2,3). \tag{2}$$

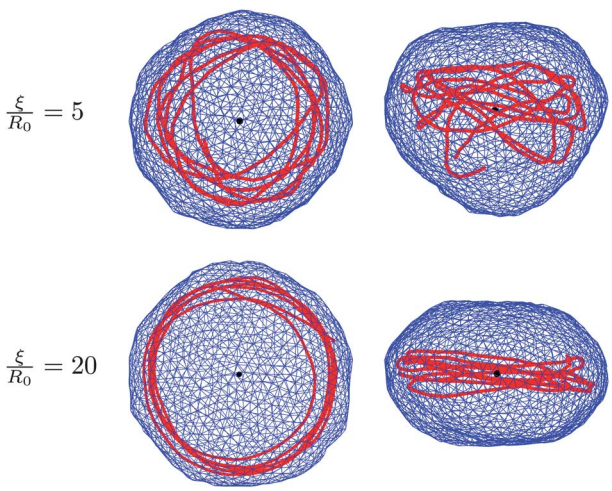

Fig. 3 Same as in Fig. 2, but for larger scaled persistence lengths ξ/R_0 of the polymer as indicated. Here, the persistence lengths are larger than the diameter $2R_0$ of the corresponding spherical vesicle. The polymer adopts the conformation of an ordered coil within a somewhat oblate-shaped vesicle.

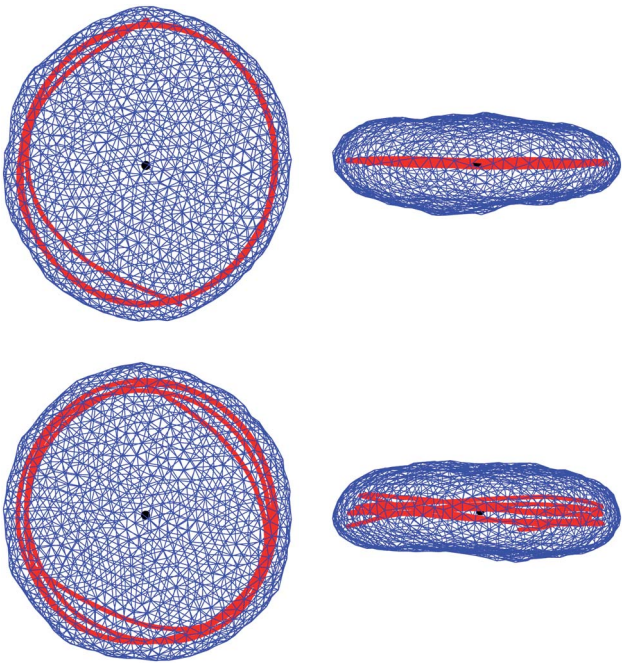

Fig. 4 Snapshots as on Fig. 2 and 3, but for a polymer with persistence length $\xi = 200R_0$, much larger then the lateral dimension of the vesicle. Upper and lower rows show, respectively, snapshots corresponding to the polymer without (as in Fig. 2 and 3) and with self-avoidance.

Here, $r_{k,i}$ is the i-th Cartesian coordinate of the position vector $\vec{r}_k$ of the k-th particle. The origin of the coordinate system is located at the center of mass and the sum runs over all particles of the object. From the principal moments (*i.e.*, the eigenvalues) $\lambda_1 \geq \lambda_2 \geq \lambda_3$ of S_{ij} (calculated using the algorithm outlined by Smith[42]), we obtain the asphericity of the object[43]

$$A = \frac{\left\langle (\lambda_1 - \lambda_3)^2 + (\lambda_2 - \lambda_3)^2 + (\lambda_1 - \lambda_2)^2 \right\rangle}{2\left\langle (\lambda_1 + \lambda_2 + \lambda_3)^2 \right\rangle} \tag{3}$$

with $\langle \ldots \rangle$ denoting ensemble averages. We point out that a one-dimensional object (where $\lambda_2 = \lambda_3 = 0$) leads to $A = 1$, a two-dimensional axisymmetric disk (where $\lambda_1 = \lambda_2$ and $\lambda_3 = 0$) entails $A = 1/4$, and a sphere (where $\lambda_1 = \lambda_2 = \lambda_3$) gives rise to $A = 0$. The asphericity A has frequently been used in the past to characterize polymers in confined geometries.[23,28,44]

We separately perform the calculation of the asphericity for the vesicle and for the polymer. The ensemble averages needed to calculate A are obtained from our Monte Carlo simulations. Specifically, after an initial equilibration of the system, the averages in eqn (3) are calculated over 10 million sweeps, where one sweep consists of separate Monte Carlo attempts to displace each of the N vertices in the membrane, followed by separate N attempts to flip a randomly chosen bond within the membrane, and followed by separate attempts to displace each of the M polymer vertices. After every 2500 sweeps gyration tensors and corresponding eigenvalues are calculated.

Fig. 5 and 6 show the asphericity of the vesicle and of the polymer, respectively, as functions of the polymer persistence length ξ, measured in units of the spherical vesicle radius R_0.

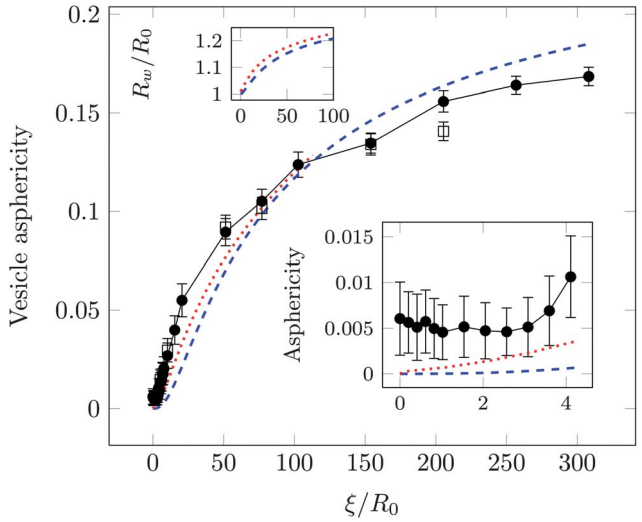

Fig. 5 Asphericity A of the vesicle as a function of the scaled persistence length ξ/R_0 of the polymer. Bars indicate standard deviations. Filled bullets and open squares correspond to a polymer, respectively, without and with self-avoidance. Results for the disk model (dashed blue line) and for the shape-optimized ground state (dotted red line) are also shown. The inset in the lower-right corner replots the vesicle asphericity within the range $0 \le \xi/R_0 \le 4$. The inset in the upper-left corner shows the vesicle's waist radius R_w (scaled by R_0) as function of ξ/R_0. (Note that R_w is defined as the radius of the circle formed by the vesicle at its plane of up-down symmetry.) Here again, dashed blue line and dotted red line correspond to disk model and optimized vesicle shape, respectively.

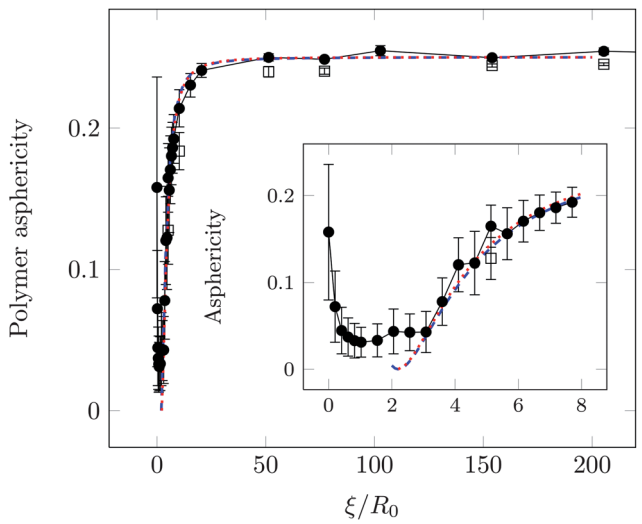

Fig. 6 Asphericity A of the polymer as a function of the scaled persistence length ξ/R_0 of the polymer. Bars indicate standard deviations. Filled bullets and open squares correspond to a polymer, respectively, without and with self-avoidance. Results for the disk model (dashed blue line) and for the shape-optimized ground state (dotted red line) are also shown. The inset replots the polymer asphericity within the range $0 \le \xi/R_0 \le 8$.

The two datasets correspond to the polymer modeled without (filled bullets) and with (open squares) self-avoidance.

The limit $\xi \to 0$ does not give rise to vanishing asphericity A, neither for the vesicle nor for the polymer. In the absence of the polymer, the fluctuation-driven deviation of the average vesicle shape from that of a perfect sphere has been analyzed recently by Linke *et al.*,[45] yet not in terms of the asymmetry parameter A. Our present Monte Carlo simulations predict $A = 0.0073$ with a standard deviation of 0.0046 for the vesicle (with bending stiffness $\kappa = 10k_BT$) in the absence of the polymer. Similarly for a bare unconstrained polymer, it is known from work by Rudnick and Gaspari[43] that the asphericity A adopts a value of 0.39. Our present simulations yield a lower value of about 0.16. This is because the radius of gyration of the polymer in the limit $\xi \to 0$ is approx. $\bar{l}\sqrt{M} \approx 1.8R_0$, indicating that the polymer is confined to some extent by the vesicle and thus adopts a smaller asphericity.

Increasing the persistence length of the polymer from zero to about $\xi/R_0 \approx 1$ slightly lowers the asphericity of both the vesicle and polymer. Our simulation data clearly indicate this for the polymer, see the inset of Fig. 6, but are somewhat less conclusive for the vesicle, see the inset of Fig. 5. Upon further increasing the persistence length ξ, the asphericity A increases. This is because the polymer starts to coil into an ordered circular structure near the vesicle membrane, thus pushing the membrane outwards and deforming the vesicle into an oblate shape. For both vesicle and polymer, the increase in A starts at the same value of $\xi/R_0 \approx 3$, indicating that the ordering transition of the polymer and the initial shape change of the vesicle are coupled. In the limit of a very stiff polymer $\xi/R_0 \gg 1$ the vesicle deforms into a thin disk with the polymer adopting an almost circular shape near its waist (see Fig. 4). Here, vesicle and polymer approach the limiting values for a thin axisymmetric object, $A = 1/4$.

To obtain a more quantitative understanding of the behavior $A = A(\xi/R_0)$ for the vesicle (Fig. 5), we have calculated its asphericity using the phenomenological models discussed in Section 2. The simplest approximation of the vesicle shape is the disk model (introduced in Section 2 and analyzed in Appendix 1); *i.e.* a flat disk with semi-toroidal rim and the polymer forming a circular ring at the waist of the vesicle; see the illustration in Fig. 1. The corresponding asphericity A for the vesicle is displayed by the dashed blue line in Fig. 5. Although the disk model makes a reasonable prediction for A, it somewhat underestimates the Monte Carlo simulation values for $\xi/R_0 < 100$ and overestimates them for $\xi/R_0 > 100$. This, in fact, is how vesicle shape fluctuations are expected to affect the asphericity: small ξ/R_0 give rise to almost spherical vesicle shapes in the ground state that fluctuations render more aspherical. Conversely, for sufficiently large ξ/R_0 the ground state will be a thin disk that out-of-plane fluctuations render more spherical. We have also calculated the asphericity based on the fully optimized vesicle ground state (as outlined in Appendix 2). Results of this calculation, which was performed in the region $0 \le \xi/R_0 \le 100$, are displayed in Fig. 5; see the dotted red line. The bending energy of the vesicle is, of course, lower for the fully optimized vesicle ground state as compared to the disk model. (Recall that Fig. 1 explicitly compares the two elastic energies.) Hence, the polymer is able to deform the vesicle more when the ground state is fully optimized, implying that the radius R_w of the circular ring the polymer forms is larger as compared to the disk model. This is confirmed by an explicit

comparison of R_w for the two models, shown in the upper-left inset of Fig. 5 (here again, the dashed blue line and the dotted red line correspond to the disk model and the fully optimized ground state, respectively). The larger waist radius R_w implies the vesicle in its fully optimized ground state to have larger asphericity – this is confirmed in Fig. 5.

We also discuss the behavior of the asphericity $A = A(\xi/R_0)$ for the polymer (Fig. 6). Ignoring fluctuations of the polymer conformation altogether would lead to a circular shaped ground state implying $A = 1/4$. To describe how $A(\xi/R_0)$ approaches this limiting value, polymer fluctuations must be accounted for. Based on scaling arguments, Odijk[46] has introduced a deflection length $l_c = R^2/\xi$ for a strongly curved semi-flexible polymer, where ξ is the polymer's persistence length and R the radius of curvature. The deflection length can be used to express the polymer's degree of orientational angular fluctuations $\langle\theta^2\rangle = \delta^2/{l_c}^2$ as $\langle\theta^2\rangle \simeq l_c/\xi$, implying a "fuzziness" of $\delta \simeq R^3/\xi^2$ of the strongly curved polymer.[46] The "fuzziness" can also be derived from minimizing the free energy of the polymer $F_p/(k_BT) \simeq (L/\xi) \times \ln(1/\delta) + \xi L/(R-\delta)^2$ with respect to δ. Here, the two contributions to F_p result, respectively, from the confinement and bending of the polymer. For $R \gg \delta$ we obtain Odijk's result $\delta \simeq R^3/\xi^2$. Let us apply this result to the polymer investigated in the present study. For large persistence length the polymer forms a ring-like structure that becomes fuzzy through in-plane and out-of-plane fluctuations. The in-plane fluctuations keep the polymer at an average distance $\delta \simeq R^3/\xi^2$ away from the waist of the vesicle. Out-of-plane fluctuations will occupy the space available to the polymer in the normal direction. Assuming the vesicle forms a sphere of radius $R_0 = R$ and $\delta \ll R_0$, the space available to the polymer in the normal direction is $w \simeq \sqrt{R_0\delta}$ (numerical prefactors are omitted). Hence, $(w/R_0)^2 \simeq \delta/R_0 \simeq (R_0/\xi)^2$. The polymer fluctuations of extension w in the normal direction give rise to a polymer asphericity

$$A = \left(\frac{\gamma(R_0/\xi)^2 - 6}{\gamma(R_0/\xi)^2 + 12}\right)^2. \quad (4)$$

Here γ is a numerical factor that we cannot determine using the present scaling-type arguments. We obtain eqn (4) based on the polymer being represented by a thin circular ribbon of length $2\pi(R_0 - \delta) \approx 2\pi R_0$ and width w, and using the relation $(w/R_0)^2 \simeq (R_0/\xi)^2$; for details see Appendix 2. The relation $A(\xi/R_0)$ is plotted in Fig. 6, see the dashed blue line, $\gamma = 30$ is chosen so as to fit the Monte Carlo simulation data best. For large ξ/R_0 the theoretical prediction somewhat underestimates the asphericity obtained from our simulations (*i.e.*, when carried out without self-avoidance of the polymer). Note that the behavior of A for small ξ/R_0 has little physical significance because neither is the condition $\delta \ll R_0$ satisfied nor is the polymer forming an ordered coil for $\delta/R_0 \lesssim 1$. It is still curious that A according to eqn (4) passes through a minimum as does the simulation result for A.

The prediction in eqn (4) is derived for a fluctuating polymer that forms a circular ring-like structure inside a spherical vesicle of radius R_0. The spherical shape of the vesicle enters as an assumption that will not be fulfilled for $\xi/R_0 \gg 1$. We can account for shape changes based on the disk model. As discussed above, the disk model represents the vesicle by a flat disk with a semi-toroidal rim. The shape of the disk can adjust so as to best accommodate the polymer (which forms a circle at the waist of the rim). There are only two modifications that the disk model introduces as compared to representing the vesicle as a sphere. First the relation $\delta = {R_0}^3/\xi^2$ is replaced by $\delta = {R_w}^3/\xi^2$ where R_w is the optimal waist radius of the vesicle according to the disk model. Second, the relation $w \approx \sqrt{R_0\delta}$ is replaced by $w \approx \sqrt{h\delta}$ where h is the thickness of the disk. When accounting for vesicle shape changes, the thin ribbon (which represents the normal fluctuations of the polymer) is inserted into the disk instead of a sphere. The disk is able to adjust its shape as function of ξ/R_0. More specifically, the two quantities R_w and h follow from minimizing the vesicle shape according to the disk model as function of ξ/R_0. The elastic energy according to the disk model is specified in Appendix 1; see eqn (7). The asphericity A of the polymer with vesicle shape changes accounted for (*i.e.*, according to the disk model) is plotted in Fig. 6; see the dotted red line. There is almost no difference, implying that vesicle shape changes have little influence on the asphericity of the polymer.

5 Conclusions

In this work we have investigated a single polymer enclosed in a fluid vesicle. Upon increasing its persistence length the polymer undergoes an ordering transition, forming a circular conformation that induces a flattening of the vesicle so as to better accommodate the polymer. Asphericity of vesicle and polymer both pass through a minimum just prior to the onset of the ordering transition; *i.e.*, when the persistence length of the polymer is roughly equal to the vesicle size. For persistence lengths much larger than that, the vesicle adopts an increasingly more oblate shape with the polymer at its waist adopting a circular conformation. Here, ground state calculations provide reasonable estimates for the vesicle shape and asphericity. The asphericity of the polymer can be rationalized in terms of Odijk's[46] deflection length. We point out that our work focuses on the simplest case, where neither interactions between membrane and polymer nor between polymer segments (other than steric) are included. For example, polymer–polymer interactions can give rise to the formation of helical structures for polymers in spherical confinement.[47] Beyond that, the present model can also be extended to account for polymer networks enclosed in fluid membranes. We also point out that the present work focuses on one single contour length of the polymer, equal to roughly five times the circumference of the nominally spherical vesicle. The theoretical models employed in the present work (mostly ground state energy calculations) apply also to longer chains. We expect them to provide reasonable descriptions for vesicles with longer chains as long as self-avoidance of the polymer can be neglected. Eventually, for sufficiently long polymers steric polymer–polymer interactions and corresponding packing constraints will become relevant.[34] This is another interesting extension of the present work. Even for a small

contour length of the polymer *i.e.*, when a stiff polymer is barely longer than the vesicle size, the vesicle may respond through shape changes that are worth future investigations.

Appendix 1: tube model and disk model

As discussed in Section 2, we use two simplified geometric models for estimating the elastic energy of the vesicle–polymer system. The *tube model* consists of a cylindrical segment of length L_c and radius R_c, which contains a polymer of contour length L forming a helical conformation. The cylinder ends are covered by two hemi-spherical caps of radius R_c. The *disk model* consists of a flat disk of thickness h and radius R_s that is capped by an semi-toroidal segment of outer radius $R_s + h$. The polymer, which has a contour length L, adopts a circular conformation of radius $R_w = R_s + h$. Vesicle and polymer are illustrated in Fig. 7 for both the tube model (left) and disk model (right). Recall that we express the (fixed) area of the vesicle $A_{ves} = 4\pi {R_0}^2$ in terms of the radius R_0 of an equivalent sphere. Also, $\xi k_B T$ and κ denote the bending rigidities of the polymer and vesicle, respectively.

We first discuss the *tube model*. The fixed area of the sphero-cylinder provides us the relation $L_c = 2R_c[(R_0/R_c)^2 - 1]$. The helical shape of the polymer can be parameterized by the position vector $\vec{r} = \{R_c\cos(\omega t), R_c\sin(\omega t), t\}$ with $\omega = \sqrt{(L/L_c)^2 - 1}\big/R_c$ and $0 \le t \le L_c$, producing a contour of length L and curvature $c = [1 - (L_c/L)^2]/R_c$. Adding the contributions from the vesicle and the enclosed polymer and using area conservation, we express the total elastic energy $E = E_{tube}$ of the vesicle–polymer system (see eqn (1)) as

$$\frac{E_{tube}}{8\pi\kappa} = \frac{3+s}{4} + \frac{ab}{8}s\left[1 - \frac{(s-1)^2}{\pi^2 b^2 s}\right]^2. \quad (5)$$

Here, we have defined dimensionless parameters

$$s = \left(\frac{R_0}{R_c}\right)^2, \quad a = \frac{\xi k_B T}{\kappa R_0}, \quad b = \frac{L}{2\pi R_0}. \quad (6)$$

The first term on the right-hand side of eqn (5) (*i.e.*, $(3 + s)/4$) is the bending energy of the vesicle, and the second term accounts for bending the polymer. Parameters a and b describe the scaled stiffness and contour length of the polymer, respectively. Our simulations correspond to $0 \le a \le 30$ and $b = 4.9$. Parameter s is unconstrained but must reside in the region $1 \le s \le s_{max}$. Here, $s = 1$ and $s = s_{max}$ correspond to $L_c = 0$ and $L_c = L$, respectively. Because for $L_c = L$ the polymer is fully stretched and thus has vanishing bending energy, we obtain from eqn (5) the expression $\pi^2 b^2 s_{max} = (s_{max} - 1)^2$ or, when solved, $s_{max} = 1 + 2(\pi b/2)^2\left(1 + \sqrt{1 + (\pi b/2)^{-2}}\right)$. For a long polymer $b \gg 1$ and therefore $s_{max} = (\pi b)^2$ or, equivalently, $A = 2\pi R_c L$. Here, the area of the two end caps becomes negligibly small as compared to the mantle of the cylinder.

The elastic energy $E_{tube}(s)$ is plotted in Fig. 8 for $b = 4.9$ (*i.e.*, corresponding to our Monte Carlo simulations). We note that $E_{tube}(s)$ exhibits a minimum at $s = 1$, indicating a spherical vesicle, and for $a > 1.2$ another minimum near $s \approx s_{max} \approx (\pi b)^2$ that corresponds to the almost fully stretched polymer. The minimum at $s = 1$ is lower than that at $s \approx s_{max}$ as long as $a < a^* = 97$. At $a = a^*$ both energy minima are separated by a large energy barrier ($\approx 2100 \times 8\pi\kappa$ for $b = 4.9$). The inset of Fig. 8 shows how a^* depends on b.

Next, we discuss the *disk model*. Here, the vesicle adopts the shape of a flat disk with a semi-toroidal rim, and the polymer forms a circle at the waist of the vesicle; see Fig. 7. The area of the vesicle has contributions from the two flat circular top and bottom segments, each equal to $\pi {R_s}^2$, and from the semi-toroidal rim, which amounts to $2\pi h(2h + \pi R_s)$. Defining the ratio $s = R_s/h$ as a measure for the deviation of the disk shape from that of a sphere ($s = 0$), area conservation of the vesicle gives rise to the relation $2 + \pi s + s^2 = 2(R_0/h)^2$. Using this relation and calculating the bending energies for the polymer and vesicle, it is straightforward to express the elastic energy $E = E_{disk}$ of the vesicle–polymer system (see eqn (1)) as

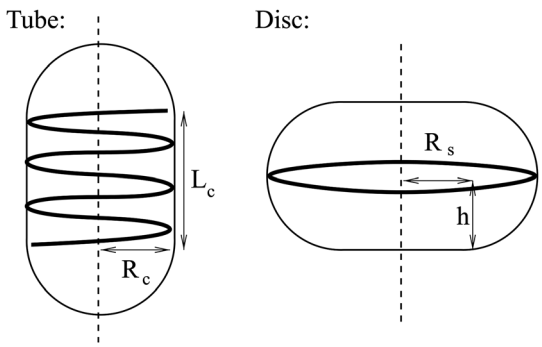

Fig. 7 Schematic illustration of two geometric models: the *tube model* (left) represents the vesicle as a sphero-cylinder of radius R_c and total length $L_c + 2R_c$ that contains the polymer in a helical conformation. The *disk model* (right) represents the vesicle by a flat disk of thickness $2h$ and radius R_s, capped by a semi-toroidal rim. Here, the polymer adopts a circular conformation of radius $R_w = R_s + h$ along the waist of the vesicle. The vertical broken line marks the axis of the vesicle's rotational symmetry.

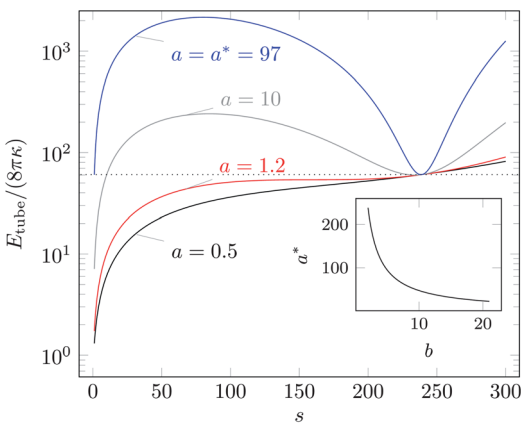

Fig. 8 Elastic energy $E_{tube}(s)$ for the tube model, plotted according to eqn (5). Different curves correspond to different $a = \xi k_B T/(\kappa R_0)$ as indicated, all derived for $b = L/(2\pi R_0) = 4.9$. Generally, $E_{tube}(s)$ exhibits two minima, one at $s = 0$ and one at $s \approx s_{max} \approx (\pi b)^2$. At $a = a^* = 97$ the two minima have the same magnitude as indicated by the dotted line. The inset shows how a^* depends on b. Note that our simulations correspond to $b = 4.9$ and cover the range $0 \le a \le 30$.

$$\frac{E_{\mathrm{disk}}}{8\pi\kappa} = 1 + \frac{s^2}{2\sqrt{1-s^2}}\operatorname{arccoth}\left(\frac{1+s}{\sqrt{1-s^2}}\right) + \frac{ab}{8}\times\frac{2+\pi s+s^2}{2(1+s)^2}, \quad (7)$$

where again $a = \xi k_{\mathrm{B}}T/(\kappa R_0)$ and $b = L/(2\pi R_0)$ as in eqn (6). The first two terms on the right-hand side of eqn (7) correspond to the bending energy of the vesicle, and the last term to the bending of the polymer. Note that E_{disk} depends only on the product ab, whereas E_{tube} depends on a and b individually. As for the sphero-cylinder, s constitutes an unconstrained degree of freedom. The elastic energy $E_{\mathrm{disk}}(s)$ adopts a single minimum for any given value of ab. This minimal value is displayed in Fig. 1 as dashed blue line, corresponding to $b = 4.9$.

Appendix 2: shape optimization

We describe the full optimization of the vesicle shape, given the vesicle has fixed area $A_{\mathrm{ves}} = 4\pi {R_0}^2$ and the polymer adopts a circular conformation of radius R_{w} at the waist of the vesicle. Consider a vesicle of axial symmetry about the z-axis and mirror symmetry about the x, y-plane, where the polymer is located. (Due to the mirror symmetry, we only need to calculate the vesicle shape for $z > 0$.) We describe the vesicle shape as a function of the contour length l of the vesicle's cross-section using the local radial distance $\rho(l)$ to the axis of symmetry and the angle $\Psi = \Psi(l)$ between the normal of the vesicle surface and the axis of symmetry (*i.e.*, the z-axis). The two functions $\rho(l)$ and $\Psi(l)$ depend on each other through $\cos\Psi = \mathrm{d}\rho/\mathrm{d}l$. The two principal curvatures of the vesicle membrane are $c_1 = \mathrm{d}\Psi/\mathrm{d}l$ and $c_2 = \sin\Psi/\rho$. Hence, the elastic energy of the vesicle–polymer system (see eqn (1)) is

$$E = 2\times 2\pi\,\frac{\kappa}{2}\int_0^{l_{\max}}\left(\frac{\mathrm{d}\Psi}{\mathrm{d}l}+\frac{\sin\Psi}{\rho}\right)^2\rho\mathrm{d}l + \frac{k_{\mathrm{B}}T\xi}{2}\frac{L}{{R_{\mathrm{w}}}^2}, \quad (8)$$

where the first and second part on the right-hand side correspond to the elastic energies of vesicle and polymer, respectively. As before, κ is the bending stiffness of the membrane, ξ is the persistence length of the polymer, and L is the contour length of the polymer. The integration runs up to a constant $l_{\max}$, which can be determined so as to satisfy conservation of the vesicle area A_{ves}. It is convenient to have the contour start at the specific radial distance R_{w} at the $z = 0$ plane and progress until reaching the z-axis. That is, at $l = 0$ and $l = l_{\max}$, the functions $\rho(l)$ and $\Psi(l)$ fulfill the conditions $\rho(0) = R_{\mathrm{w}}$, $\rho(l_{\max}) = 0$, $\Psi(0) = \pi/2$, and $\Psi(l_{\max}) = 0$. These relations serve as boundary conditions for a set of differential equations obtained from functional minimization of $E = E[\rho(l), \Psi(l)]$; see Fošnarič *et al.*[48] for an explicit specification of the differential equations. The waist radius R_{w} can be viewed as a fixed constant for any specific calculation of E. Carrying such a calculation out for different R_{w} allows us to compute the elastic energy E as function of R_{w}. The minimum of that function then yields the optimal waist radius R_{w} and corresponding minimal elastic energy $E = E_{\min}$. The scaled optimal energy $E_{\min}/(8\pi\kappa)$ is plotted in Fig. 1 for fixed $L/(2\pi R_0) = 4.9$; see the black thick solid line. Corresponding cross-sections of vesicle shapes are also displayed in Fig. 1 for a number of specific values $\xi k_{\mathrm{B}}T/(\kappa R_0)$.

From the parameterization of the vesicle in terms of $\rho(l)$ and $z(l) = -\sin\Psi(t)$ we can calculate the asphericity (as defined in eqn (3)) through

$$A = \left(\frac{\int_{-l_{\max}}^{l_{\max}}\mathrm{d}l\rho\sqrt{\rho'^2+z'^2}\left(\rho^2/2-z^2\right)}{\int_{-l_{\max}}^{l_{\max}}\mathrm{d}l\rho\sqrt{\rho'^2+z'^2}\left(\rho^2+z^2\right)}\right)^2, \quad (9)$$

where the prime denotes the derivative; *i.e.*, $\rho' = \mathrm{d}\rho/\mathrm{d}l$ and $z' = \mathrm{d}z/\mathrm{d}l$. In Fig. 5, the results of A for the disk model (dashed blue line) and for the shape-optimized (dotted blue line) ground state model are computed using eqn (9), in each case based on the corresponding set of functions $\rho(l)$ and $z(l)$. Eqn (4) is also obtained from eqn (9) with the specific choices $\rho(l) = R_0$, $z(l) = l$, and $l_{\max} = {R_0}^2/(2\xi)$.

Acknowledgements

The authors acknowledge the support of the Slovenian Research Agency through grant no. BI-US/12-13-049.

References

1 D. Marenduzzo, C. Micheletti and E. Orlandini, *J. Phys.: Condens. Matter*, 2010, **22**, 283102.
2 V. Noireaux, Y. Maeda and A. Libchaber, *Proc. Natl. Acad. Sci. U. S. A.*, 2011, **108**, 3473–3480.
3 W. Reisner, J. N. Pedersen and R. H. Austin, *Rep. Prog. Phys.*, 2012, **75**, 106601.
4 J. A. Speir and J. E. Johnson, *Curr. Opin. Struct. Biol.*, 2012, **22**, 65–71.
5 A. Meller, *J. Phys.: Condens. Matter*, 2003, **15**, R581–R607.
6 D. Branton, D. W. Deamer, A. Marziali, H. Bayley, S. A. Benner, T. Butler, M. D. Ventra, S. Garaj, A. Hibbs, X. H. Huang, S. B. Jovanovich, P. S. Krstic, S. Lindsay, X. S. S. Ling, C. H. Mastrangelo, A. Meller, J. S. Oliver, Y. V. Pershin, J. M. Ramsey, R. Riehn, G. V. Soni, V. Tabard-Cossa, M. Wanunu, M. Wiggin and J. A. Schloss, *Nat. Biotechnol.*, 2008, **26**, 1146–1153.
7 H. Kumar, Y. Lansac, M. A. Glaser and P. K. Maiti, *Soft Matter*, 2011, **7**, 5898–5907.
8 R. B. Schoch, J. Y. Han and P. Renaud, *Rev. Mod. Phys.*, 2008, **80**, 839–883.
9 M. D. Graham, *Annu. Rev. Fluid Mech.*, 2011, **43**, 273–298.
10 D. Boal, *Mechanics of the Cell*, Cambridge University Press, 2nd edn, 2012.
11 I. Nemhauser, J. Joseph-Silverstein and W. Cohen, *J. Cell. Biol.*, 1983, **96**, 979–989.
12 W. Cohen, Y. Sorokina and I. Sanchez, *Cell Motil. Cytoskeleton*, 1998, **40**, 238–248.
13 H. Hägerstrand, M. Danieluk, M. Bobrowska-Hägerstrand, T. Holmström, V. Kralj-Iglič, C. Lindqvist and M. Nikinmaa, *Mol. Membr. Biol.*, 1999, **16**, 195–204.
14 M. Turner, R. Briehl, F. Ferrone and R. Josephs, *Phys. Rev. Lett.*, 2003, **90**, 128103.

15 D. K. Fygenson, J. F. Marko and A. Libchaber, *Phys. Rev. Lett.*, 1997, **79**, 4497–4500.
16 L. Limozin and E. Sackmann, *Phys. Rev. Lett.*, 2002, **89**, 168103.
17 D. Merkle, N. Kahya and P. Schwille, *ChemBioChem*, 2008, **9**, 2673–2681.
18 A. Viallat, J. Dalous and M. Abkarian, *Biophys. J.*, 2004, **86**, 2179–2187.
19 K. Takiguchi, A. Yamada, M. Negishi, Y. Tanaka-Takiguchi and K. Yoshikawa, *Langmuir*, 2008, **24**, 11323–11326.
20 M. Elbaum, D. K. Fygenson and A. Libchaber, *Phys. Rev. Lett.*, 1996, **76**, 4078–4081.
21 M. M. A. E. Claessens, R. Tharmann, K. Kroy and A. R. Bausch, *Nat. Phys.*, 2006, **2**, 186–189.
22 C. Micheletti, D. Marenduzzo and E. Orlandini, *Phys. Rep.*, 2011, **504**, 1–73.
23 K. Ostermeir, K. Alim and E. Frey, *Phys. Rev. E: Stat., Nonlinear, Soft Matter Phys.*, 2010, **81**, 061802.
24 M. Fritsche and D. W. Heermann, *Soft Matter*, 2011, **7**, 6906–6913.
25 P. Cifra and T. Bleha, *Macromol. Theory Simul.*, 2012, **21**, 15–23.
26 M. R. Smyda and S. C. Harvey, *J. Phys. Chem. B*, 2012, **116**, 10928–10934.
27 A. Cacciuto and E. Luijten, *Nano Lett.*, 2006, **6**, 901–905.
28 S. Jorge and A. Rey, *J. Chem. Phys.*, 1997, **106**, 5720–5730.
29 L. Livadaru and H. J. Kreuzer, *New J. Phys.*, 2003, **5**, 95.
30 G. Morrison and D. Thirumalai, *J. Chem. Phys.*, 2005, **122**, 194907.
31 A. J. Spakowitz and Z. G. Wang, *Phys. Rev. Lett.*, 2003, **91**, 166102.
32 G. Morrison and D. Thirumalai, *Phys. Rev. E: Stat., Nonlinear, Soft Matter Phys.*, 2009, **79**, 011924.
33 F. Brochard-Wyart, T. Tanaka, N. Borghi and P. G. de Gennes, *Langmuir*, 2005, **21**, 4144–4148.
34 D. Marenduzzo and E. Orlandini, *Europhys. Lett.*, 2007, **80**, 48004.
35 G. Gompper and D. M. Kroll, in *Statistical Mechanics of Membranes and Surfaces*, ed. D. Nelson, T. Piran and S. Weinberg, World Scientific, Singapore, 2004, pp. 359–426.
36 G. Gompper and D. M. Kroll, *J. Phys. I*, 1996, **6**, 1305–1320.
37 W. Helfrich, *Z. Naturforsch.*, 1973, **28**, 693–703.
38 S. Pronk, P. Geissler and D. Fletcher, *Phys. Rev. Lett.*, 2008, **100**, 258102.
39 N. Ramakrishnan, P. B. S. Kumar and J. H. Ipsen, *Macromol. Theory Simul.*, 2011, **20**, 446–450.
40 E. Cerda and L. Mahadevan, *Proc. R. Soc. A*, 2005, **461**, 671–700.
41 V. Romero, T. A. Witten and E. Cerda, *Proc. R. Soc. A*, 2008, **464**, 2847–2866.
42 O. K. Smith, *Commun. ACM*, 1961, **4**, 168.
43 J. Rudnick and G. Gaspari, *Science*, 1987, **237**, 384–389.
44 M. B. Luo, J. H. Huang and J. M. Xu, *Polym. J.*, 1998, **30**, 889–890.
45 G. T. Linke, R. Lipowsky and T. Gruhn, *Phys. Rev. E: Stat., Nonlinear, Soft Matter Phys.*, 2005, **71**, 051602.
46 T. Odijk, *Macromolecules*, 1993, **26**, 6897–6902.
47 Z. Y. Yang, D. Zhang, L. X. Zhang, H. P. Chen, W. Ateeq-ur-Rehman and H. J. Liang, *Soft Matter*, 2011, **7**, 6836–6843.
48 M. Fošnarič, A. Iglič, D. M. Kroll and S. May, *J. Chem. Phys.*, 2009, **131**, 105103.

